Available online at www.sciencedirect.com
ScienceDirect
Journal of Organometallic Chemistry 692 (2007) 3167–3173
Journal of Organometallic Chemistry
www.elsevier.com/locate/jorganchem

# Spin density distribution in mononuclear Rh(0) complexes: A combined experimental and DFT study

Bas de Bruin [a,*], Jaap C. Russcher [b], Hansjörg Grützmacher [c,*]

[a] Universiteit van Amsterdam, Faculty of Science, van't Hoff Institute for Molecular Sciences (HIMS), Department of Homogeneous and Supramolecular Catalysis, Nieuwe Achtergracht 166, Room B.925, 1018 WV Amsterdam, The Netherlands
[b] Radboud University Nijmegen, Faculty of Science, Institute for Molecules and Materials, Nijmegen, The Netherlands
[c] Department of Chemistry and Applied Biosciences, ETH Zürich, CH-8093 Zürich, Switzerland

Received 7 December 2006; received in revised form 18 January 2007; accepted 18 January 2007
Available online 30 January 2007

**Abstract**

The paramagnetic complex $[Rh(trop_2dach)]^{\bullet}$ **2** was obtained by reduction of the almost planar 16-electron cationic precursor complex, $[Rh(trop_2dach)]^{+}$ **1** and characterized by EPR spectroscopy [$g_{11} = 2.069$, $g_{22} = 2.014$, $g_{33} = 1.964$, $g_{iso} = 2.016$; $A(Rh) = (<40, 29, 30)$]. The unobservable small nitrogen hyperfine coupling and DFT calculations show that most of the spin density is localized on the hydrocarbon ligand framework and only about 35% on the metal center. DFT calculations on various 17 electron rhodium complexes with carbonyl, olefine, or phosphane ligands like $[Rh(CO)_4]^{\bullet}$, $[Rh(cod)_2]^{\bullet}$, and $[Rh(dppe)_2]^{\bullet}$ reveal that in none of these the spin density at the metal center exceeds 45%. That is all formally Rh(0) complexes reported to date are better described as highly delocalized radicals and an assignment of the formal metal oxidation state is not meaningful.


*Keywords:* EPR spectroscopy; DFT calculations; Redox chemistry; Rhodium; Olefin complexes; Amine complexes

## 1. Introduction

For more than 30 years, paramagnetic mononuclear rhodium complexes in which a $d^9$ valence electron configuration is assigned to the Rh center have been studied with various ligand types like CO [1], olefins like cyclooctadiene (cod) [2], and phosphanes [3]. Most of these compounds were only electrochemically generated and are rather short lived intermediates. Only a few complexes were isolated ($[Rh(PF_3)_4]^{\bullet}$ [3c], $[Rh\{P(OiPr)_3\}_4]^{\bullet}$ [3e]) and structurally characterized ($[Rh(dppf)_2]^{\bullet}$ [4], $[Rh\{bis(tropp)\}]^{\bullet}$ [5], $[Rh(tropp)_2]^{\bullet}$ [6]; dppf = 1,1′-(*di*p*h*enyl*p*hosphino)*f*errocene, for the other complexes see Scheme 1). Mononuclear zerovalent rhodium complexes have been proposed as reactive intermediates in C–H activation chemistry [7] and photocatalytic $H_2O$ splitting [8]. More recent work indicated that not the radicals are the ultimate reactive species but their diamagnetic disproportionation products formed in the equilibrium, $2\,[Rh(L)_n]^{\bullet} \leftrightarrow [Rh(L)_n]^{+} + [Rh(L)_n]^{-}$ [3e,9].

Complexes with "non-innocent" ligands like 2,2′-bipyridine or phenanthroline derivatives [10] or macrocyclic ligands with unsaturated phosphorus heterocycles (especially strong π-acceptors) [11] were also studied.

We reported the synthesis of the neutral $[Rh(trop_2dad)]^{\bullet}$ radical (Scheme 1) ($trop_2dad$ = 1,4-bis(5H-dibenzo[a,d]-cyclohepten-5-yl)-1,4-diazabuta-1,3-diene) [12]. This complex is especially stable. A detailed EPR investigation combined with DFT calculations clearly showed that the unpaired electron is predominantly delocalized over the "non-innocent" ligand framework and this complex is best described as a [16 + 1] electron complex in which the $trop_2dad^{\bullet -}$ radical anion is coordinated to a $d^8$–Rh(I) center.

Given that we have shown that olefins can likewise behave as "non-innocent" ligands in paramagnetic Rh(II)

* Corresponding authors. Tel.: +41 1 632 2855; fax: +41 1 632 1090 (H. Grützmacher).
*E-mail addresses:* bdebruin@science.uva.nl (B. de Bruin), gruetzmacher@inorg.chem.ethz.ch (H. Grützmacher).

0022-328X/$ - see front matter © 2007 Elsevier B.V. All rights reserved.
doi:10.1016/j.jorganchem.2007.01.041

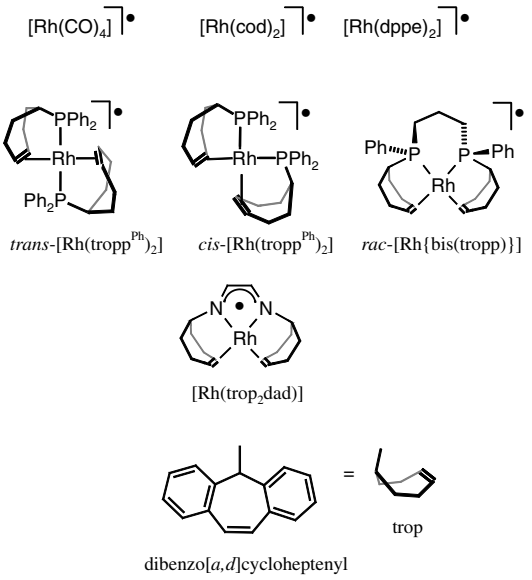


Scheme 1. Formally zerovalent rhodium complexes reported in the literature so far.

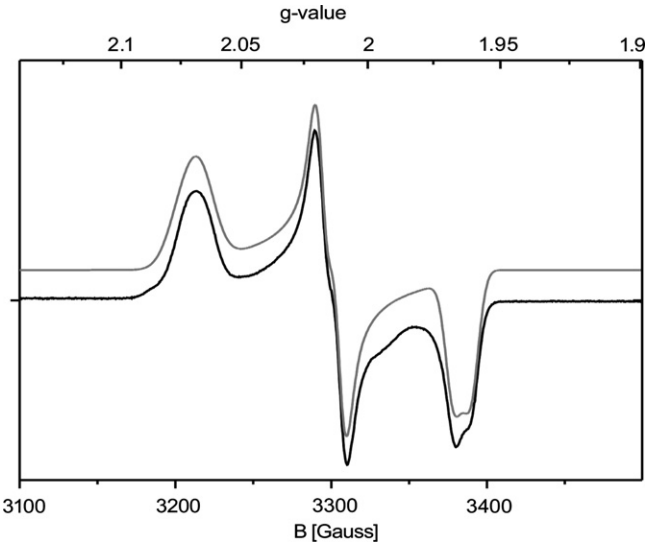


Fig. 1. Experimental and simulated EPR spectrum of $[Rh(trop_2dach)]^{\bullet}$ (2) at X-band (9.303044 GHz) at $T = 68$ K.

and Ir(II) complexes [13], we became interested in the question in how far an olefinic binding site behaves "non-innocently" in Rh(0) complexes. To address this question, we investigated the reduction of the cationic 16 electron di(amino) di(olefin) complex $[Rh(trop_2dach)]^{+}$ to the corresponding radical $[Rh(trop_2dach)]^{\bullet}$. This radical is especially well suited for our purpose because amines behave as very weak π-acceptors and hence do not compete with the olefinic groups. Additionally we performed DFT calculations for representative carbonyl, olefin, and phosphane Rh(0) complexes and show that a "true" Rh(0) complex remains to be synthesized.

## 2. Results and discussion

### 2.1. EPR spectroscopy

Reaction of the $PF_6$ salt of the red cationic 16 electron complex $[Rh(trop_2dach)]^{+}$ (**1**) [14], with sodium naphtalenide in THF containing 0.1 M $nBu_4NPF_6$ gave a deep red solution of the neutral 17 electron complex $[Rh(trop_2dach)]^{\bullet}$ (**2**), see Scheme 2. After 5 min., the reaction mixture was cooled to 77 K (liquid nitrogen) and then to 68 K in the EPR spectrometer. Apart from helping a better glass formation of the frozen solvent, the ammonium salt enhanced significantly the stability of the radical **2**.

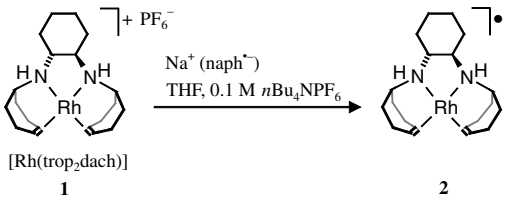


Scheme 2. Synthesis of the $[Rh(trop_2dach)]^{\bullet}$ radical complex **2**.

The continuous wave (CW) EPR spectrum of the frozen solution at X-band is shown in Fig. 1.

A satisfactorily fit was obtained by simulating the experimental spectrum with $g_1 = 2.069$, $g_2 = 2.014$, $g_3 = 1.964$ and the $^{103}Rh$ hyperfine couplings $A_2(Rh) = 29$ MHz and $A_3(Rh) = 30$ MHz. Neither the hyperfine coupling $A_1(Rh)$ at the low-field end of the spectrum nor the nitrogen couplings $A(N)$ were resolved indicating that the latter must be very small (see Table 2). This may be taken as a first hint that the spin population at the nitrogen atoms is small as anticipated.

### 2.2. DFT calculations

In order to gain a more detailed picture of the electronic structure of the various paramagnetic rhodium complexes mentioned above, DFT calculations were performed. The structures of $[Rh(CO)_4]^{\bullet}$ (Fig. 2a), $[Rh(cod)_2]^{\bullet}$ (Fig. 2b), and *p*-$[Rh(dppe)_2]^{\bullet}$ with a planar structure (Fig. 2c), *t*-$[Rh(dppe)_2]^{\bullet}$ with a tetrahedral structure (Fig. 2d), *cis*- and *trans*-$[Rh(tropp^{Ph})_2]^{\bullet}$ (Fig. 2e and f), the *R*,*R*-stereoisomer of $[Rh\{bis(tropp)\}]^{\bullet}$ (Fig. 2g), the diazadiene complex $[Rh(trop_2dad)]^{\bullet}$ (Fig. 2h), and the bisamino radical complex $[Rh(trop_2dach)]^{\bullet}$ **2** (Fig. 2i) were optimized with the TURBOMOLE program package. Selected bond lengths and angles are listed in Table 1.

Neither a planar nor a tetrahedral structure is expected for a $d^9$–$[ML_4]$ complex. In the first case, the unpaired electron would occupy a strongly anti-bonding and destabilizing orbital composed with the metal $d_{x^2-y^2}$ orbital while a tetrahedral structure would undergo a Jahn–Teller-(JT)-distortion. Indeed our calculations predict distorted structures of $D_{2d}$ symmetry for the global minimum structures of $[Rh(CO)_4]^{\bullet}$, $[Rh(cod)_2]^{\bullet}$, and $[Rh(dppe)_2]^{\bullet}$. The degree of distortion can be expressed by the intersection angle $\Phi$ which is defined by the planes running

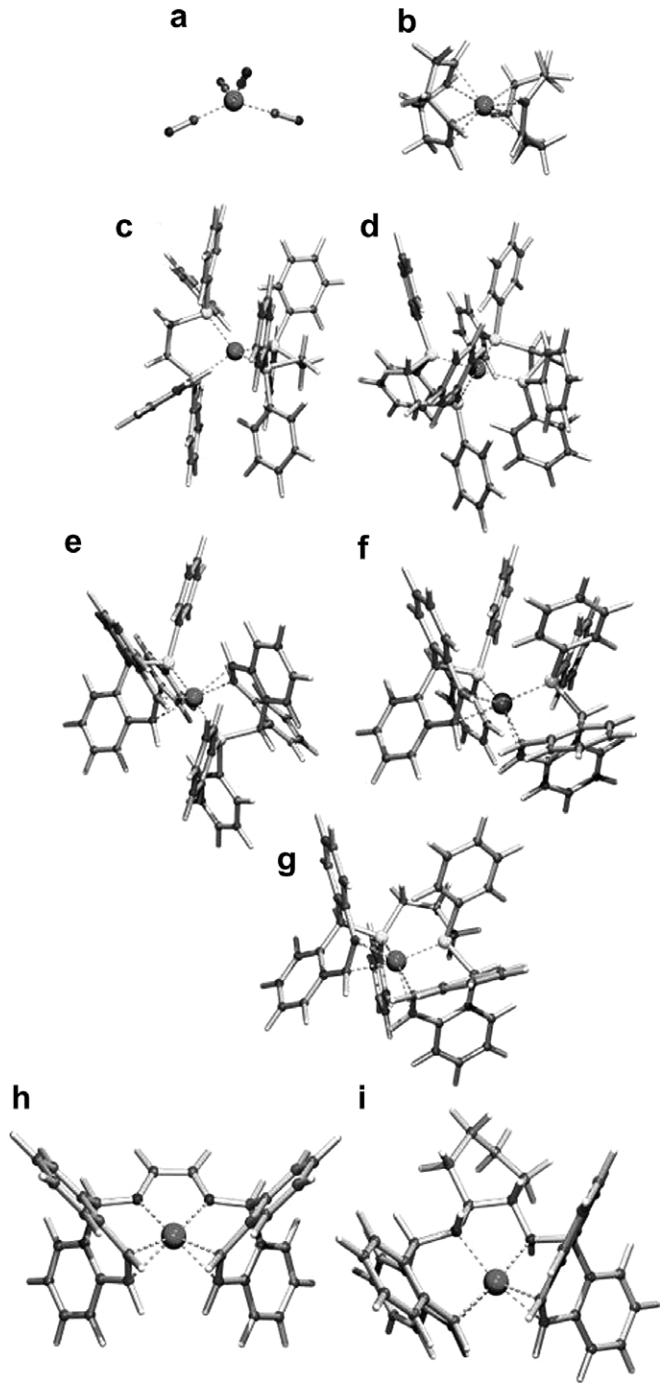


Fig. 2. Calculated structures of $[Rh(CO)_4]^{\bullet}$ (a), $[Rh(cod)_2]^{\bullet}$ (b), *t*-$[Rh(dppe)_2]^{\bullet}$ (c), *p*-$[Rh(dppe)_2]^{\bullet}$ (d), *trans*-$[Rh(tropp^{Ph})_2]^{\bullet}$ (e), *cis*-$[Rh(tropp^{Ph})_2]^{\bullet}$ (f), *R,R*-$[Rh\{bis(tropp)\}]^{\bullet}$ (g), $[Rh(trop_2dad)]^{\bullet}$ (h), and $[Rh(trop_2dach)]^{\bullet}$ (i).

through the donor atoms of each ligand and the metal center. In case of olefins as ligands, we use the centroid, ct, of the coordinated C=C double bond. In an ideal tetrahedron, the angles $\Phi$ between two such planes are always 90°, whereas in an ideal planar geometry such angles are 0°, irrespective of which ligands are chosen to define the planes.

For geometries "in between", the angle between two such planes depends on which ligands are chosen to define these planes, but the *smallest* angle $\Phi$ is a good measure to indicate the extend of distortion (distorted square planar: 0–44°; distorted tetrahedral: 46–90°). These intersection angles $\Phi$ are listed in Table 1. For $[Rh(dppe)_2]$ we find two local minima. One minimum structure, *p*-$[Rh(dppe)_2]^{\bullet}$, has a slightly distorted square planar geometry ($\Phi = 5.9°$) of approx. $D_{4h}$ symmetry, the other, *t*-$[Rh(dppe)_2]^{\bullet}$, shows a strongly distorted tetrahedral geometry ($\Phi = 60°$) of approx. $C_2$ symmetry. The tetrahedral complex *t*-$[Rh(dppe)_2]^{\bullet}$ is more stable by $\Delta E = 24$ kJ mol$^{-1}$ (based on single point calculations at the b3-lyp/TZVP level). Note that a tetrahedrally distorted structure has been observed experimentally (X-ray diffraction) for $[Rh(dppf)_2]^{\bullet}$ [4] with $\Phi = 75.2°$ while both a tetrahedral structure [3e] and a planar structure was suggested for $[Rh\{P(OiPr)_3\}_4]^{\bullet}$ [3f]. Likewise, the diphosphine diolefin complexes *cis*-$[Rh(tropp^{Ph})_2]^{\bullet}$ and *R,R*-$[Rh\{bis(tropp)\}]^{\bullet}$ have structures which lie rather precisely half-way between a planar and tetrahedral structure ($\Phi_{exp} = 43°$; $\Phi_{calc} = 44.4°$). For *trans*-$[Rh(tropp^{Ph})_2]^{\bullet}$ we calculate a structure closer to a planar one ($\Phi_{exp} = 29.4°$). Experimentally, the structure is unknown for the rhodium complex but was determined for the iridium analogue, *trans*-$[Ir(tropp^{Ph})_2]^{\bullet}$, by a single crystal X-ray diffraction study which gave $\Phi_{exp} = 33.8°$ [15]. Also for the diamine diolefin complex $[Rh(trop_2dach)]^{\bullet}$ **2**, a tetrahedrally distorted structure is predicted by the DFT calculations $\Phi_{calc} = 34.4°$. Only, for the $[Rh(trop_2dad)]^{\bullet}$ radical an almost ideally planar structure is calculated ($\Phi = 0.06°$). This is expected, because the $[Rh(trop_2dad)]$ complex bears almost no spin density at Rh (spin population 0.1%), and this compound is best described as a Rh(I)-ligand radical species $[Rh(I)(trop_2dad^{\bullet-})]$. Generally, the calculated structures agree very well with the ones experimentally determined. The somewhat longer metal–ligand bond lengths for the calculated structures are typically found with the bp86/SV(P) DFT level of theory [16].

May one conclude inversely that the strongly distorted tetrahedral structures for the other metallo-radicals indicate that these are best described as $d^9$–Rh(0) complexes? In Table 2 we list the calculated EPR parameters for the compounds discussed here. Spin populations for these complexes are listed in Table 3.

The calculated *g*-tensors are in excellent agreement with the experimentally determined tensors. The calculated absolute hyperfine couplings are slightly smaller than the experimental values which, however, may be a result of the assumption made in the interpretation of the experimental spectra that the hyperfine and *g*-tensors coincide. This might also explain the apparent different experimental and calculated principle hyperfine tensor components in some cases. Similar arguments may apply for the slight deviation of the experimental from the calculated values for the P-hyperfine couplings. Clearly, the small anisotropy of the *g*-tensor ($\Delta g = g_1 - g_3$) ranging from 0.011 in

Table 1
Geometrical parameters for experimental and DFT calculated $Rh^0$ complexes

| | Rh–E (Å) (exp.) | Rh–E (Å) (DFT) | Rh–ct (Å) (exp.)[a] | Rh–ct (Å) (DFT)[a] | C=C (Å) (exp.) | C=C (Å) (DFT) | $\Phi$ (°)[b] (exp.) | $\Phi$ (°)[b] (DFT) |
|---|---|---|---|---|---|---|---|---|
| $[Rh(CO)_4]^{\bullet}$ | – | 1.943[c] | – | – | – | – | – | 52.4[f] |
| $[Rh(cod)_2]^{\bullet}$ | – | – | – | 2.089 | – | 1.422 | – | 44.4 |
| E = P | | | | | | | | |
| *p*-$[Rh(dppe)_2]^{\bullet}$ | – | 2.353[d] | – | – | – | – | – | 5.9[g] |
| *t*-$[Rh(dppe)_2]^{\bullet}$ | – | 2.332[d] | – | – | – | – | – | 60.0[g] |
| *cis*-$[Rh(tropp^{Ph})_2]^{\bullet}$ | 2.270 | 2.323[d] | 2.107 | 2.112 | 1.418 | 1.444 | 43[f] | 44.4[h] |
| *trans*-$[Rh(tropp^{Ph})_2]^{\bullet}$ | – | 2.212[d] | – | 2.111 | – | 1.451 | – | 29.4[h] |
| $[Rh\{bis(tropp)\}]^{\bullet}$ | 2.231 | 2.277[d] | 2.084 | 2.106 | 1.413 | 1.444 | 43[f] | 42.4[h] |
| E = N | | | | | | | | |
| $[Rh(trop_2dad)]^{\bullet}$ | – | 2.020[e] | – | 2.046 | – | 1.438 | – | 0.06[i] |
| $[Rh(trop_2dach)]^{\bullet}$ | – | 2.182[e] | – | 2.009 | – | 1.456 | – | 34.4[i] |

E denotes the heteroelement bonded to the metal center (E = P in entries 3–7, E = N in entries 8–9).
[a] Average of the two/four distances from Rh to the centroids, ct, of the C=C bonds.
[b] Smallest angle between the planes {$L_1$, $L_2$, Rh} and {$L_1$, $L_2$, Rh}.
[c] Average of the four Rh–C distances.
[d] Average of the two or four Rh–P distances.
[e] Average of the two Rh–N distance.
[f] Planes running through Rh and two inequivalent (*non*-symmetry related) CO ligands.
[g] Defined by the planes running through the chelate ring dppe P atoms and Rh.
[h] Defined by the planes running through the chelate ring P, Rh and the centroid of the C=C bond.
[i] Defined by the planes running through the chelate ring N, Rh and the centroid of the C=C bond.

Table 2
Experimental and DFT calculated EPR parameters of the $Rh^0$ complexes

| | $g_{11}$ | $g_{22}$ | $g_{33}$ | $g_{iso}$ | $A_{11}$(Rh) | $A_{22}$($^{103}$Rh) | $A_{33}$($^{103}$Rh) | $A_{iso}$($^{103}$Rh) | $A_{11}$(E) | $A_{22}$(E) | $A_{33}$(E) | $A_{iso}$(E) |
|---|---|---|---|---|---|---|---|---|---|---|---|---|
| $[Rh(CO)_4]^{\bullet}$ | 2.015 | 2.002[b] | 2.002[b] | 2.006 | <15 | 24[a] | 24[a] | 21 | – | – | – | – |
| *Calc.* | *2.045* | *2.000* | *2.000* | *2.015* | *23* | *22* | *7* | *17* | – | – | – | – |
| $[Rh(cod)_2]^{\bullet}$ | 2.056 | 2.019 | 2.016 | 2.030 | ≈50[c] | ≈42 | (nr)[c] | – | – | – | – | – |
| *Calc.* | *2.049* | *2.027* | *2.018* | *2.031* | *21* | *21* | −5 | *12* | – | – | – | – |
| E = P | | | | | | | | | | | | |
| *p*-$[Rh(dppe)_2]^{\bullet}$ | – | – | – | 2.027 | – | – | – | – | – | – | – | 146 |
| *Calc.* | *2.004* | *1.997* | *1.946* | *1.982* | *16* | *12* | *12* | *13* | 71 | 78 | 121 | 90 |
| *t*-$[Rh(dppe)_2]^{\bullet}$ | – | – | – | – | – | – | – | – | – | – | – | – |
| *Calc.* | *2.022* | *2.009* | *2.005* | *2.012* | *11* | *11* | *11* | *11* | *93* | *104* | *148* | *115* |
| *cis*-$[Rh(tropp^{Ph})_2]^{\bullet}$ | 2.03 | 2.013 | 2.019 | 2.021 | 20 | 16 | 17 | 18 | 80 | 65 | 70 | 72 |
| *Calc.* | *2.031* | *2.012* | *2.011* | *2.018* | *18* | *13* | −2 | *10* | *45* | *52* | *93* | *63* |
| *trans*-$[Rh(tropp^{Ph})_2]^{\bullet}$ | 2.05 | 2.037 | 2.03 | 2.039 | 23 | 20 | 19 | 21 | 55 | 45 | 40 | 47 |
| *Calc.* | *2.048* | *2.039* | *2.005* | *2.031* | 0 | −18 | −36 | −18 | *17* | *21* | *43* | 27 |
| $[Rh\{bis(tropp)\}]^{\bullet}$ | – | – | – | 2.0208 | – | – | – | – | – | – | – | 84 |
| *Calc.* | *2.03* | *2.02* | *2.014* | *2.028* | *16* | *14* | −4 | *9* | *57* | *64* | *105* | *76* |
| E = N | | | | | | | | | | | | |
| $[Rh(trop_2dad)]^{\bullet}$ | 2.011 | 1.998 | 1.998 | 2.002 | −0.01 | −0.21 | 6 | −3.5 | 0.9 | 0.9 | 34 | 11.9 |
| *Calc.* | 2.013 | 2.011 | 1.999 | *2.008* | *9.2* | *8.5* | −8.5 | *4* | −3.3 | −1.3 | *29.5* | *7.7* |
| $[Rh(trop_2dach)]^{\bullet}$ | 2.069 | 2.014 | 1.964 | 2.016 | (<40) nr[c] | 29 | 30 | – | – | – | – | – |
| *Calc.* | *2.054* | *2.018* | *1.964* | *2.012* | *37* | *14* | −1 | *17* | −5.1 | −3.1 | *1.7* | *0.2* |

E denotes the heteroelement bonded to the metal center (E = P in entries 3–7, E = N in entries 8–10)[a].
[a] Hyperfine couplings are in MHz.
[b] Reported as $g_{\perp}$ and $A_{\perp}$.
[c] nr = not resolved.

*cis*-$[Rh(tropp^{Ph})_2]^{\bullet}$ to 0.105 in the newly synthesized $[Rh(trop_2dach)]^{\bullet}$ and isotropic *g* values close to the one of the free electron ($g_e = 2.0023$) speak against a $d^9$–Rh(0) description [17]. On the other hand, the corresponding cobalt complex $[Co(tropp^{Ph})_2]$ shows a significantly larger *g*-anisotropy ($\Delta g = 0.24$). Inspection of the hyperfine couplings with other nuclei in the ligand ($^{31}P$, $^{14}N$, $^{13}C$, $^{1}H$) shows these to be likewise inconspicuous [6a].

Table 3
Spin populations $\rho$ of selected rhodium complexes

| | | $\rho$ (Rh) (%) (exp.) | $\rho$ (Rh) (%) (DFT) | $\rho$ (E) (%) (exp.) | $\rho$ (E) (%) (DFT) | $\rho$ (C) (%) (exp.) | $\rho$ (C) (%) (DFT) | $\rho$ (C) (%)[a] (DFT) | $\rho$ (C) (%)[b] (DFT) | $\rho$ (C) (%)[c] (DFT) | $\rho$ (C) (%)[d] (DFT) |
|---|---|---|---|---|---|---|---|---|---|---|---|
| 1 | $[Rh(CO)_4]^{\bullet}$ | <40 | *45* | – | – | ~4 | *4 × 10* | – | – | – | |
| 2 | $[Rh(cod)_2]^{\bullet}$ | – | *25* | – | – | – | – | *2 × 20* | *2 × 20* | – | |
| | | | | *E = P* | | | – | – | – | – | |
| 3 | *p*-$[Rh(dppe)_2]^{\bullet}$ | – | *20* | – | *4 × 12* | – | – | – | – | – | |
| 4 | *t*-$[Rh(dppe)_2]^{\bullet}$ | – | *35* | – | *4 × 11* | – | – | – | – | – | |
| 5 | *cis*-$[Rh(tropp^{Ph})_2]^{\bullet}$ | 2–5[e] | *29* | 2 × ~5[b] | *2 × 7* | ~0.5[e] | – | *2 × 18* | *2 × 0* | *2 × (6, 6, 8)* | *2 × (−3, −3, −3)* |
| 6 | *trans*-$[Rh(tropp^{Ph})_2]^{\bullet}$ | – | *29* | – | *2 × 6* | – | – | *2 × 18* | *2 × 0* | *2 × (5, 5, 7)* | *2 × (−2, −2, −3)* |
| 7 | $[Rh\{bis(tropp)\}]^{\bullet}$ | – | *24* | – | *2 × 8* | – | – | *2 × 18* | *2 × 0* | *2 × (6, 6, 8)* | *2 × (−3, −3, −3)* |
| | | | | *E = N* | | | | | | | |
| 8 | $[Rh(trop_2dad)]^{\bullet}$ | – | *0.1* | *2 × 22.5* | *2 × 22* | – | *2 × 18*[f] | *2 × 3.4* | *2 × 3.4* | *4 × (1, 1, 2)* | |
| 9 | $[Rh(trop_2dach)]^{\bullet}$ | – | *36* | – | *2 × 1* | – | – | *2 × 15* | *2 × 0* | *2 × (7, 7, 11)* | *2 × (−3, −3, −2)* |

DFT values are given in italics.
[a] $C^1$ (olefinic).
[b] $C^2$ (olefinic).
[c] $\rho$ *on the two ortho*-carbons and one *para*-carbon of the benzo groups.
[d] $\rho$ *on the two meta*-carbons and one *ipso*-carbon of the benzo groups.
[e] Tentatively estimated.
[f] α-Diimine carbons.

Table 3 lists the calculated spin population on the rhodium center and selected ligand atoms. With the exception of the $[Rh(trop_2dad)]^{\bullet}$ complex which is clearly a Rh(I) tropdad$^{\bullet-}$ radical anion complex by all spectroscopic and theoretical means, the electronic structures of the other species are more complicated, with spin populations at Rh ranging from 20% to 45%. None of these compounds should be regarded as true Rh(0) $d^9$ metal centered radicals nor as Rh(I) complexes of ligand centered radicals.

The high degree of delocalization of the unpaired spin density is demonstrated in the plots of the spin density distribution which we show for $[Rh(trop_2dach)]^{\bullet}$ **2** as a representative (Fig. 3). As we anticipated, there is very little spin population on the nitrogen atoms ($\rho \approx 1\%$). Actually, the unpaired electron is largely delocalized over the two trop moieties. For each trop fragment the spin is delocalized over *one olefinic carbon atom* ($\rho = 15\%$) and *one* benzo group which is adjacent to this spin carrying olefinic carbon center. Each of the two benzo moieties of the delocalized system carries a total of about 25% of the spin population at the two *ortho*-and the *para*-carbon centers. This amounts to 80% total *positive* spin population at the ligand compared to only 36% at the metal (~16% *negative* spin population at the *ipso* and *meta* carbons of the same benzo moieties compensates for the ~16% excess of total *positive* spin population at the metal and ligand fragments).

A $C_2$ symmetric distribution of the spin density is expected in view of the symmetry of the molecule. It is, however, striking that the spin density resides only on one of the olefinic carbon atoms and its neighbouring benzo moiety (both in *trans*-position with respect to the adjacent N–H function of one tropNH part of the ligand) [18]. Such an unequal distribution of the spin density with the ligand backbone has also been observed in a complex with a formal Rh(II) center and a trop type ligand system [19]. Only 36% of the odd electron is located at the rhodium center of **2**.

The distribution of the spin population is very similar in the other rhodium trop phosphane complexes (see entries 5–7 in Table 3 and Scheme 3), with the slight difference that the spin population is even smaller at the rhodium center.

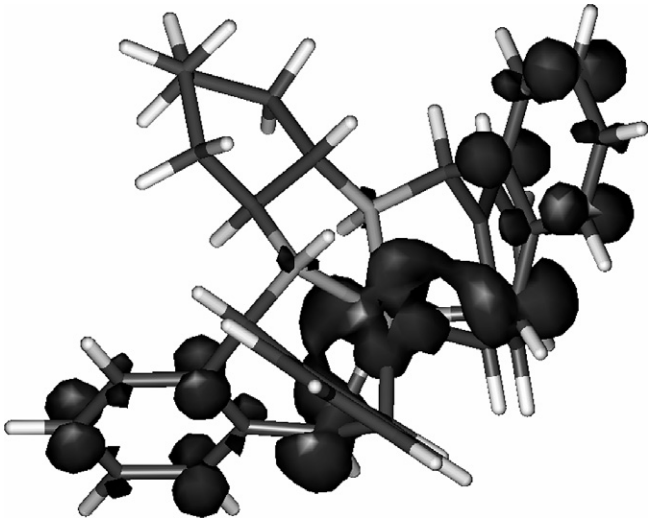

Fig. 3. Plot of the spin density of the $[Rh(trop_2dach)]^{\bullet}$ radical (Turbomole b3-lyp/TZVP).

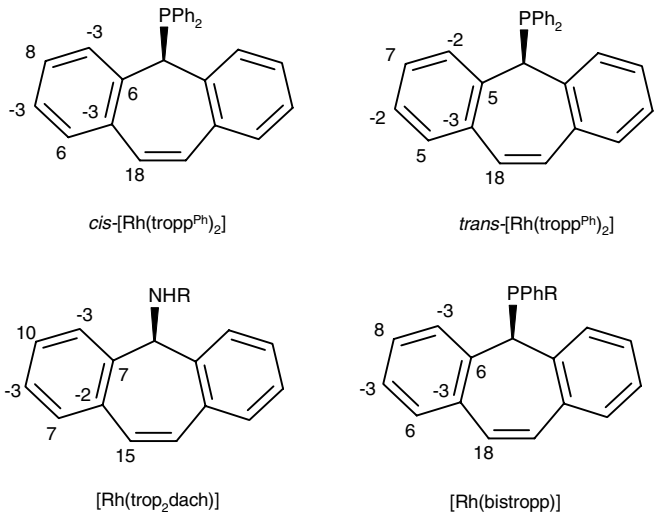


Scheme 3. Unsymmetrical spin population distribution over the "redox non-innocent" trop moieties of the formally Rh(0) complexes.

This is easily explained by the larger π-acceptor strength of phosphanes compared to amines. Remarkably (and may be counter-intuitively) the largest spin population at the rhodium center is calculated for the carbonyl species $[Rh(CO)_4]^{\bullet}$ ($\rho = 45\%$) although the CO group is commonly regarded as a strong π-acceptor. On the other hand, CO is a strong σ-donor as well and a small molecule thereby restricting delocalization simply by size. The significantly smaller spin population at Rh in $[Rh(cod)_2]^{\bullet}$ ($\rho = 25\%$) when compared to *t*-$[Rh(dppe)_2]^{\bullet}$ ($\rho = 35\%$) is expected in view of the comparatively strong π-acceptor/weak σ-donor capability of olefins when compared to phosphanes which act as strong σ-donors but weak π-acceptors.

## 3. Conclusions

The radical $[Rh(trop_2dach)]^{\bullet}$ **2** containing two amine σ-donor and two olefin π-acceptor functions in *trans*-position of a strongly tetrahedrally distorted coordination sphere is sufficiently stable in a 0.1 M solution of $nBu_4NPF_6$ in THF to be characterized by CW EPR spectra. These data, in combination with DFT calculations, show that very little spin density resides on the nitrogens and also only 36% is found on the rhodium center. The major part of the spin density is delocalized over the hydrocarbon framework of the trop ligand system. Inspection of previously reported monomeric rhodium complexes with carbonyl, olefin, and/or phosphane ligands show that none of these can be described as a true $d^9$–Rh(0) complex; in all of them the odd electron is highly delocalized. This is likely due to the fact that all ligands applied so far have energetically low lying π-type acceptor orbitals which interact strongly with the d-orbitals at the metal. Evidently, this enhances the stability of the formally zerovalent rhodium complexes and lowers the reduction potential of the cationic precursor complexes, but a truly rhodium centered metallo-radical in which the majority of the spin density is localized on the metal center remains to be synthesized and its reactivity to be studied.

## 4. Experimental section

Experimental X-band EPR spectra were recorded on a Bruker ER220 spectrometer. The spectra were simulated by iteration of the anisotropic *g* values, (super)hyperfine coupling constants, and line widths. We thank Dr. F. Neese (MPI Strahlenchemie Mülheim a/d Ruhr) for a copy of his EPR simulation program.

The EPR spectrum of $[Rh(trop_2dach)]^{\bullet}$ complex **4** was obtained by chemical reduction of the $PF_6^-$ salt of its cationic $Rh^I$ precursor $[Rh(trop_2dach)]^+$ with sodium naphtalenide in THF containing 0.1 M $[(nBu)_4N]PF_6$. Five minutes after addition of the reducing agent, the reaction mixture was quenched in liquid $N_2$, and further cooled to 68 K in the EPR cryostat.

### 4.1. DFT geometry optimizations and EPR parameter calculations

All geometry optimizations were carried out with the Turbomole program [20a,20b] coupled to the PQS Baker optimizer [21]. Geometries were fully optimized as minima at the bp86 [22] level using the Turbomole SV(P) basisset [20c,20d] on all atoms (small-core pseudopotential [20c,20e] on Rh). Improved energies and spin density plots were obtained from single-point calculations at the b3-lyp level [23] using the TZVP basis [20c,20f] (small-core pseudopotential [20c,20e] on Rh). EPR parameters [24] were calculated with the ADF [25] program system using the bp86 [22] functional with the ZORA/TZP basis sets supplied with the program (all electron, core double zeta, valence triple zeta polarized basis set on all atoms), using the coordinates from the structures optimized in Turbomole as input.

## 5. Supporting information

Coordinates (XYZ and PDB format) of the rhodium species in optimized geometries (Turbomole, bp86/SV(P)). EPR parameter listings (*g*-tensors, *A*-tensors for all atoms) obtained by EPR properties calculations (ADF). This information is available upon request from the authors.

## Acknowledgements

This work was supported by the Netherlands Organization for Scientific Research (NWO-CW), the Radboud University of Nijmegen and the University of Amsterdam, the Swiss National Science Foundation (SNF), and the ETH Zürich. We thank Dr. Peter H.M. Budzelaar (University of Manitoba) for helpful tips and tricks concerning the DFT calculations.

## References


[1] J.H.B. Chenier, M. Histed, J.A. Howard, H.A. Jolly, H. Morris, B. Mile, Inorg. Chem. 28 (1989) 4114.

[2] (a) E. Makrtik, J. Hanzlik, A. Camus, J. Organomet. Chem. 142 (1) (1977) 95;
(b) J. Orsini, W.E. Geiger, J. Electroanal. Chem. 380 (1995) 83.

[3] (a) A complete reference list cannot be given here, for selected literature see and references cited therein: D.C. Olson, W. Keim, Inorg. Chem. 9 (1969) 2028;
(b) J.F. Nixon, B. Wilkins, D.A. Clement, J. Chem. Soc., Dalton Trans. (1974) 1993;
(c) M.A. Bennett, R.N. Johnson, T.W. Turney, Inorg. Chem. 15 (1976) 2938;
(d) L. Horner, K. Dickerhof, J. Mathias, Phosphorus Sulfur 10 (1981) 349;
(e) G.N. George, S.I. Klein, J.F. Nixon, Chem. Phys. Lett. 108 (1984) 627;
(aa) A.J. Kunin, E.J. Nanni, R. Eisenberg, Inorg. Chem. 24 (1985) 1852;
(f) G. Pilloni, G. Zotti, S. Zecchin, J. Organomet. Chem. 317 (1986) 357;
(g) G.C. Johnston, M.C. Baird, J. Organomet. Chem. 314 (1986) C51;
(h) B. Bogdanovic, W. Leitner, C. Six, U. Wilczok, K. Wittmann, Angew. Chem., Int. Ed. Engl. 36 (1997) 502.

[4] B. Longato, R. Coppo, G. Pilloni, C. Corvaja, A. Toffoletti, G. Bandoli, J. Organomet. Chem. 710 (2001) 637.

[5] C. Laporte, F. Breher, F. Geier, J. Harmer, A. Schweiger, H. Grützmacher, Angew. Chem., Int. Ed. 43 (2004) 2567.

[6] (a) H. Schönberg, S. Boulmaâz, M. Wörle, L. Liesum, A. Schweiger, H. Grützmacher, Angew. Chem., Int. Ed. 37 (1998) 1423;
(b) S. Deblon, L. Liesum, J. Harmer, H. Schönberg, A. Schweiger, H. Grützmacher, Chem. Eur. J. 8 (3) (2002) 601.

[7] J.A. Sofranko, R. Eisenberg, J.A. Kampmeier, J. Am. Chem. Soc. 102 (1980) 1163.

[8] (a) S. Oishi, J. Mol. Catal. 39 (1987) 225;
(b) E. Amouyal, in: M. Chanon (Ed.), Homogeneous Photocatalysis, vol. 2, Wiley, New York, 1997, p. 264.

[9] (a) S. Deblon, H. Rüegger, H. Schönberg, S. Loss, V. Gramlich, H. Grützmacher, New J. Chem. 23 (2001) 83;
(b) F. Breher, H. Rüegger, M. Mlakar, M. Rudolph, S. Deblon, S. Boulmaâz, H. Schönberg, J. Thomaier, H. Grützmacher, Chem. Eur. J. 10 (2004) 641.

[10] (a) H. Căldăraru, K. DeArmond, K.W. Hanck, Y.Em. Sahini, J. Am. Chem. Soc. 98 (1976) 4455;
(b) W.A. Fordyce, K.H. Pool, G.A. Crosby, Inorg. Chem. 21 (1982) 1027.

[11] L. Cataldo, S. Choua, T. Berclaz, M. Geoffroy, N. Mézailles, N. Avarvari, F. Mathey, P. Le Floch, J. Chem. Phys. A 106 (2002) 3017.

[12] F. Breher, C. Böhler, G. Frison, J. Harmer, L. Liesum, A. Schweiger, H. Grützmacher, Chem. Eur. J. 9 (2003) 3859.

[13] (a) D.G.H. Hetterscheid, B. de Bruin, Eur. J. Inorg. Chem. (2007) 211;
(b) D.G.H. Hetterscheid, M. Klop, R.J.N.A.M. Kicken, J.M.M. Smits, E.J. Reijerse, B. de Bruin, Chem. Eur. J. (in press);
(c) D.G.H. Hetterscheid, J. Kaiser, E. Reijerse, T.P.J. Peters, S. Thewissen, A.N.J. Blok, J.M.M. Smits, R. de Gelder, B. de Bruin, J. Am. Chem. Soc. 127 (2005) 1895;
(d) D.G.H. Hetterscheid, M. Bens, B. de Bruin, Dalton Trans. (2005) 979;
(e) D.G.H. Hetterscheid, J.M.M. Smits, B. de Bruin, Organometallics 23 (2004) 4236;
(f) D.G.H. Hetterscheid, B. de Bruin, J.M.M. Smits, A.W. Gal, Organometallics 22 (2003) 3022;
(g) B. de Bruin, S. Thewissen, T.-W. Yuen, T.P.J. Peters, J.M.M. Smits, A.W. Gal, Organometallics 21 (2002) 4312;
(h) B. de Bruin, T.P.J. Peters, S. Thewissen, A.N.J. Blok, J.B.M. Wilting, R. de Gelder, J.M.M. Smits, A.W. Gal, Angew. Chem., Int. Ed. 41 (2002) 2135;
(aa) B. de Bruin, T.P.J. Peters, S. Thewissen, A.N.J. Blok, J.B.M. Wilting, R. de Gelder, J.M.M. Smits, A.W. Gal, Angew. Chem. 114 (2002) 2239.

[14] P. Maire, F. Breher, H. Schönberg, H. Grützmacher, Organometallics 24 (2005) 3207.

[15] S. Boulmaâz, M. Mlakar, S. Loss, H. Schönberg, S. Deblon, M. Wörle, R. Nesper, H. Grützmacher, Chem. Commun. (1998) 2623.

[16] T. Ziegler, J. Autschbach, Chem. Rev. 105 (2005) 2695.

[17] (a) D.G.H. Hetterscheid, A.J.J. Koekkoek, H. Grützmacher, Bas de Bruin, Prog. Inorg. Chem. 55 (in press);
(b) B.A. Goodman, J.B. Raynor, Electron spin resonance of transition metal complexes, in: H.J. Emeléus, A.G. Sharpe (Eds.), Advances in Inorganic Chemistry and Radiochemistry, vol. 13, 1970, p. 136.

[18] The unequal distribution of electron density over the two benzo groups of each tropNH moiety of the ligand is also observed in the energetically lower lying orbitals which are involved in the metal to ligand backbonding (for details see the Supporting Information).

[19] P. Maire, S. Anandaram, T. Büttner, J. Harmer, I. Gromov, H. Rüegger, F. Breher, A. Schweiger, H. Grützmacher, Angew. Chem., Int. Ed. Engl. 45 (2006) 3265.

[20] (a) R. Ahlrichs, M. Bär, H.-P. Baron, R. Bauernschmitt, S. Böcker, M. Ehrig, K. Eichkorn, S. Elliott, F. Furche, F. Haase, M. Häser, C. Hättig, H. Horn, C. Huber, U. Huniar, M. Kattannek, A. Köhn, C. Kölmel, M. Kollwitz, K. May, C. Ochsenfeld, H. Öhm, A. Schäfer, U. Schneider, O. Treutler, K. Tsereteli, B. Unterreiner, M. von Arnim, F. Weigend, P. Weis, H. Weiss, Turbomole Version 5, Theoretical Chemistry Group, University of Karlsruhe, 2002;
(b) O. Treutler, R. Ahlrichs, J. Chem. Phys. 102 (1995) 346;
(c) Turbomole basisset library, Turbomole Version 5, see a;
(d) A. Schäfer, H. Horn, R. Ahlrichs, J. Chem. Phys. 97 (1992) 2571;
(e) D. Andrae, U. Haeussermann, M. Dolg, H. Stoll, H. Preuss, Theor. Chim. Acta 77 (1990) 123;
(f) A. Schäfer, C. Huber, R. Ahlrichs, J. Chem. Phys. 100 (1994) 5829.

[21] (a) PQS version 2.4, 2001, Parallel Quantum Solutions, Fayetteville, Arkansas, USA (the Baker optimizer is available separately from PQS upon request);
(b) J. Baker, J. Comput. Chem. 7 (1986) 385.

[22] (a) A.D. Becke, Phys. Rev. A 38 (1988) 3098;
(b) J.P. Perdew, Phys. Rev. B 33 (1986) 8822.

[23] (a) C. Lee, W. Yang, R.G. Parr, Phys. Rev. B 37 (1988) 785;
(b) A.D. Becke, J. Chem. Phys. 98 (1993) 1372;
(c) A.D. Becke, J. Chem. Phys. 98 (1993) 5648;
(d) All calculations were performed using the Turbomole functional "b3-lyp", which is not identical to the Gaussian "B3LYP" functional.

[24] Lead reference for calculation of *g*-tensor (Zeeman interactions) parameters: (a) E. van Lenthe, A. van der Avoird, P.E. S Wormer, J. Chem. Phys. 107 (1997) 2488;
Lead reference for calculation of *A*-tensor (Nuclear magnetic dipole hyperfine interactions) parameters: (b) E. van Lenthe, A. van der Avoird, P.E.S. Wormer, J. Chem. Phys. 108 (1998) 4783.

[25] ADF2004.01. (a) E.J. Baerends, D.E. Ellis, P. Ros, Chem. Phys. 2 (1973) 41;
(b) L. Versluis, T. Ziegler, J. Chem. Phys. 88 (1988) 322;
(c) G. te Velde, E.J. Baerends, J. Comput. Phys. 99 (1) (1992) 84;
(d) C. Fonseca Guerra, J.G. Snijders, G. te Velde, E.J. Baerends, Theor. Chem. Acc. 99 (1998) 391.